Reprinted from ANNALS OF PHYSICS
Vol. 216, No. 2, June 1992
Printed in Belgium

Chaos in a Spin–Boson System: Classical Analysis

M. A. M. DE AGUIAR* AND K. FURUYA*

Instituto de Física "Gleb Wataghin,"
Departamento de Física do Estado Sólido e Ciências de Materiais,
Universidade de Campinas, C.P. 6165, Campinas, Brazil

C. H. LEWENKOPF†

Max-Planck-Institut für Kernphysik,
W-6900 Heidelberg, Germany

AND

M. C. NEMES*

Instituto de Física, Departamento de Física-Matemática,
Universidade de São Paulo, C.P. 20516, São Paulo, Brazil

Received November 12, 1991

We have found novel aspects of the spin–boson system in a fully classical analysis of the system. The finiteness of the spin phase space is shown to strongly influence the systematic behaviour of periodic orbits. We also give a detailed account of the consequences of the chaotic dynamics and of the superradiant phase transition. © 1992 Academic Press, Inc.

1. INTRODUCTION

In order to understand the behaviour of atoms coupled to a classical radiation field many investigations have been performed in the last four decades. Fast development in experimental studies as well as in technological applications give an additional motivation for further theoretical investigations. Since the full quantum mechanical description of this system given by the Dicke Maser model [1], much work has been devoted to the construction of its classical analogue [2–4]. In the classical framework Arecchi *et al.* [5] were the first to observe chaotic motion in

* Partially supported by CNPq, FINEP, and FAPESP.
† Supported by CNPq-Brazil.

0003-4916/92 $9.00

this interacting spin–boson system. On the other hand, more recently, full quantum mechanical calculations showed this system to exhibit typical manifestations of classical chaos [6, 7]. Chaos and its implications is the main target of this paper.

In this work we set up the corresponding classical Hamiltonian by means of coherent states for both spin and boson (or particle) degrees of freedom and report on the novel aspects brought on by the spin. One essential difference between boson and spin phase spaces is that the latter is finite. This has consequences for the structure of the periodic orbits and tori; the first will be the main point of our analysis. In order to exploit such differences a numerical method capable of handling periodic orbits for generic analytic Hamiltonians (not only of the form $H = \mathbf{p}^2/2m + V(\mathbf{q})$) is needed. We therefore develop an extension of the method by Baranger *et al.* [8]. Another interesting feature of the Maser model is its well-known superradiant phase transition. In the classical limit such transition can be viewed as bifurcations of equilibria with a simple geometrical interpretation in phase space [9].

In terms of periodic orbits we show that such bifurcations introduce a new family of periodic orbits with very distinct features of the previous one. Generally speaking we also find that the presence of classical chaos tends to introduce deformation on the corresponding stable periodic orbits. The amount of distortion clearly depends on the strength of the nonintegrable term. Also the stable regions in all families of periodic orbits diminish considerably when chaos is increased. The effect of the finiteness of the spin phase space (which we call border effect) is present in both integrable and nonintegrable regimes. We show that the border has a strong influence on the systematic behaviour of the periodic orbits as a function of increasing energy. Specifically, the families which cover large enough energy ranges show the following behaviour: as the spin projection of the periodic orbits approach the border of the spin phase space the rate of increase of the mean radius of such orbits with the energy becomes very slow, whereas the opposite occurs with the particle projection.

Investigation of the classical limit of spin–boson coupled systems in terms of periodic orbits is still far from being complete. We believe that this detailed numerical study is an important step towards a thorough understanding of such systems and hope that better understanding of the classical phase space will bring some new insights for the quantum mechanical problem.

The structure of the paper is as follows: In Section 2 we obtain the classical Hamiltonian of the Maser model, using standard coherent state techniques. In Section 3 the bifurcations of equilibria are presented in both integrable and nonintegrable limits. Section 4 contains the exact numerical solutions and linear analysis of the equations of motion. Generalization of the numerical method in [8] is described in Appendix A for the sake of clarity. Finally, our conclusions are presented in Section 5.

2. The Classical Hamiltonian

The simplest quantum system which realizes the Dicke Maser model is given by

$$\hat{H} = \varepsilon a^{\dagger} a + \varepsilon J_z + \frac{G}{\sqrt{N}}(aJ_+ + a^{\dagger}J_-) + \frac{G'}{\sqrt{N}}(a^{\dagger}J_+ + aJ_-), \tag{1}$$

where $a^{\dagger}$, a are the Bose operators of the quantized radiation mode with frequency ε. The spin operators represent $N \geqslant 2J$ (J is the total spin) two-level atoms with separation energy ε, couled to spin J and J_+, J_- are the usual $SU(2)$ raising and lowering operators corresponding to total spin J and J_z, its z-component.

The classical limit of this model is unique and a rigorous proof of its existence has been given in Ref. [2]. Therefore we use the normalized coherent states representation in order to obtain the classical Hamiltonian (we use $\hbar = 1$)

$$H_{\mathrm{cl}}(z, \bar{z}, w, \bar{w}) \equiv \langle zw|\, \hat{H}\, |zw\rangle. \tag{2}$$

The coherent states $|zw\rangle$ are defined as

$$|zw\rangle = |z\rangle \otimes |w\rangle, \tag{3}$$

where $|z\rangle$ represents the usual boson coherent state (for the Weyl group)

$$|z\rangle = e^{-z\bar{z}/2} e^{za^{\dagger}}\, |0\rangle \tag{4}$$

with $|0\rangle$ being the harmonic oscillator ground state; $|w\rangle$ is the Bloch state associated with the $SU(2)$ group [10],

$$|w\rangle = (1 + w\bar{w})^{-J} e^{wJ_+}\, |J - J\rangle, \tag{5}$$

with $|J-J\rangle$ the state with spin J and $J_z = -J$. In this manner, the following relations hold:

$$\begin{aligned} \langle z|\, a\, |z\rangle &= z \\ \langle z|\, a^{\dagger}\, |z\rangle &= \bar{z} \end{aligned} \tag{6}$$

$$\langle w|\, J_+\, |w\rangle = \frac{2J\bar{w}}{1 + w\bar{w}} \tag{7}$$

$$\langle w|\, J_-\, |w\rangle = \frac{2Jw}{1 + w\bar{w}}$$

$$\langle w|\, J_z\, |w\rangle = -J\left(\frac{1 - w\bar{w}}{1 + w\bar{w}}\right).$$

The classical analogue of the Dicke Hamiltonian is then obtained by substituting (1) into (2) and using (6) and (7):

$$H_{\mathrm{cl}} = \varepsilon z\bar{z} - \varepsilon J\left(\frac{1 - w\bar{w}}{1 + w\bar{w}}\right) + \frac{\sqrt{2J}}{1 + w\bar{w}}\left[G(\bar{w}z + w\bar{z}) + G'(wz + \bar{w}\bar{z})\right]. \tag{8}$$

The classical equations of motion [11] below follow straightforwardly,

$$\begin{aligned}
\dot{z} &= -\imath \frac{\partial H_{\mathrm{cl}}}{\partial \bar{z}} \\
\dot{\bar{z}} &= \imath \frac{\partial H_{\mathrm{cl}}}{\partial z} \\
\dot{w} &= -\imath \Omega^{-1} \frac{\partial H_{\mathrm{cl}}}{\partial \bar{w}} \\
\dot{\bar{w}} &= \imath \Omega^{-1} \frac{\partial H_{\mathrm{cl}}}{\partial w},
\end{aligned} \tag{9}$$

where

$$\Omega = 2J/(1 + w\bar{w})^2. \tag{10}$$

It is convenient to define real canonical variables in the classical study. For the particle degree of freedom the action and angle variables I_2, θ_2 are defined as usual by

$$z = \sqrt{I_2}\, e^{\imath\theta_2}. \tag{11}$$

For the spin coordinates, on the other hand, the most natural way is to relate J_z with I_1 as

$$-J\left(\frac{1 - w\bar{w}}{1 + w\bar{w}}\right) \equiv I_1 .$$

In terms of these new real variables, the classical Hamiltonian reads

$$H_{\mathrm{cl}}(\mathbf{I}, \boldsymbol{\theta}) = \varepsilon(I_1 + I_2) + \frac{2\sqrt{J^2 - I_1^2}\sqrt{I_2}}{\sqrt{2J}} [G \cos(\theta_1 - \theta_2) + G' \cos(\theta_1 + \theta_2)]. \tag{12}$$

Note that this expression could be obtained immediately from the quantum Hamiltonian by the naive substitutions

$$\begin{aligned}
\hat{a} &\to Z = \sqrt{I_2}\, e^{\imath\theta_2} \\
\hat{a} &\to \bar{Z} = \sqrt{I_2}\, e^{-\imath\theta_2} \\
\hat{J}_z &\to I_1 = J \cos \varphi_1 \\
\hat{J}_x &\to \sqrt{J^2 - I_1^2} \cos \theta_1 = J \sin \varphi_1 \cos \theta_1 \\
\hat{J}_y &\to \sqrt{J^2 - I_1^2} \sin \theta_1 = J \sin \varphi_1 \sin \theta_1
\end{aligned} \tag{13}$$

with φ_1, θ_1, the usual polar and azimuthal angle, respectively. Finally, we make a last change of variables to go from action-angle to cartesian coordinates,

$$\begin{aligned} q_1 &= \sqrt{2(J+I_1)}\sin\theta_1 \\ p_1 &= \sqrt{2(J+I_1)}\cos\theta_1 \\ q_2 &= \sqrt{2I_2}\sin\theta_2 \\ p_2 &= \sqrt{2I_2}\cos\theta_2; \end{aligned} \tag{14}$$

the variables q_2, p_2 are the usual cartesian coordinates of a harmonic oscillator. The quantities q_1, p_1 do not have a direct physical interpretation and are related to the projections J_x, J_y by $J_y/J_x = q_1/p_1$. Note that J_x and J_y do not form a pair of canonical variables.

The transformation from the original $(w, \bar{w})$ to (q_1, p_1) and $(z, \bar{z})$ to (q_2, p_2) is the following

$$\begin{aligned} p_1 &= \sqrt{J/(1+w\bar{w})}\,(w+\bar{w}) \\ q_1 &= \sqrt{J/(1+w\bar{w})}\left(\frac{w-\bar{w}}{\iota}\right) \\ p_2 &= \sqrt{\tfrac{1}{2}}\,(z+\bar{z}) \\ q_2 &= \sqrt{\tfrac{1}{2}}\left(\frac{z-\bar{z}}{\iota}\right). \end{aligned} \tag{15}$$

These equations do not constitute a canonical transformation. Indeed, the Poisson brackets give

$$\begin{aligned} [q_1, p_1]_{w\bar{w}} &= \frac{\partial q_1}{\partial w}\frac{\partial p_1}{\partial \bar{w}} - \frac{\partial p_1}{\partial w}\frac{\partial q_1}{\partial \bar{w}} = \frac{1}{\iota}\,\Omega \\ [q_2, p_2]_{z\bar{z}} &= \frac{\partial q_2}{\partial z}\frac{\partial p_2}{\partial \bar{z}} - \frac{\partial p_2}{\partial z}\frac{\partial q_2}{\partial \bar{z}} = \frac{1}{\iota} \end{aligned} \tag{16}$$

which are just the factors needed to turn Eqs. (9) into the usual Hamilton's equations,

$$\begin{aligned} \dot{p}_1 &= \frac{\partial H_{\mathrm{cl}}}{\partial q_1} \\ \dot{q}_1 &= -\frac{\partial H_{\mathrm{cl}}}{\partial p_1} \\ \dot{p}_2 &= \frac{\partial H_{\mathrm{cl}}}{\partial q_2} \\ \dot{q}_2 &= -\frac{\partial H_{\mathrm{cl}}}{\partial p_2} \end{aligned} \tag{17}$$

with

$$H_{\rm cl}(\mathbf{q},\mathbf{p}) = \frac{\varepsilon}{2}(p_1^2 + p_2^2 + q_1^2 + q_2^2) - J\varepsilon + \frac{\sqrt{4J - (p_1^2 + q_1^2)}}{\sqrt{4J}}(G_+ p_1 p_2 + G_- q_1 q_2) \quad (18)$$

and

$$\begin{aligned} G_+ &\equiv G + G' \\ G_- &\equiv G - G'. \end{aligned} \quad (19)$$

The Hamiltonian $H_{\rm cl}$ written in this representation will be the target of our study in what follows.

3. Bifurcation of Equilibria

The first step in an analytical study of a classical Hamiltonian system is the search for points of equilibrium, i.e., points where the Hamiltonian flux is zero. Writing the equations of motion explicitly we obtain

$$\dot{q}_1 = -\varepsilon p_1 - \frac{G_+ p_2 \sqrt{2J - H_1}}{\sqrt{2J}} + \frac{p_1}{2\sqrt{2J}\sqrt{2J - H_1}}(G_+ p_1 p_2 + G_- q_1 q_2) \quad (20)$$

$$\dot{p}_1 = \varepsilon q_1 + \frac{G_- q_2 \sqrt{2J - H_1}}{\sqrt{2J}} - \frac{q_1}{\sqrt{2J}\sqrt{2J - H_1}}(G_+ p_1 p_2 + G_- q_1 q_2) \quad (21)$$

$$\dot{q}_2 = -\varepsilon p_2 - \frac{G_+ p_1 \sqrt{2J - H_1}}{\sqrt{2J}} \quad (22)$$

$$\dot{p}_2 = \varepsilon q_2 + \frac{G_- q_1 \sqrt{2J - H_1}}{\sqrt{2J}}, \quad (23)$$

where

$$H_1 = \tfrac{1}{2}(p_1^2 + q_1^2).$$

When the l.h.s. is put equal to zero and p_2 and q_2 are substituted in the terms of p_1 and q_1 (using (22) and (23)), one obtains

$$q_1\left[\varepsilon - \frac{G^2\,(2J - H_1)}{2J\varepsilon} + \frac{G_+^2 p_1^2}{4J\varepsilon} + \frac{G_-^2 q_1^2}{4J\varepsilon}\right] = 0 \quad (24)$$

$$p_1\left[\varepsilon - \frac{G_+^2 (2J - H_1)}{2J\varepsilon} + \frac{G_+^2 p_1^2}{4J\varepsilon} + \frac{G_-^2 q_1^2}{4J\varepsilon}\right] = 0 \quad (25)$$

$$q_2 = -\frac{G_- q_2 \sqrt{2J - H_1}}{\varepsilon\sqrt{2J}} \quad (26)$$

$$p_2 = -\frac{G_+ p_1 \sqrt{2J - H_1}}{\varepsilon\sqrt{2J}}. \quad (27)$$

The origin $q_1 = p_1 = q_2 = p_2 = 0$ is a trivial solution of Eqs. (24)–(27). The analysis of other extrema, or equilibrium points, will depend strongly on whether G' is zero or not. Therefore, we study each case separately and put them together afterwards.

(A) $G' = 0$

In this case, $G_+ = G_- = G$ and, when the origin is discarded, Eqs. (24) and (25) degenerate. Solving for q_1^2 in terms of p_1^2 gives

$$q_1^2 = \frac{4J(G^2 - \varepsilon^2) - 2p_1^2 G^2}{2G^2}. \tag{28}$$

In order to have real solutions, $q_1^2 > 0$ and

$$p_1^2 < \frac{4J(G^2 - \varepsilon^2)}{2G^2}. \tag{29}$$

Again, to ensure that $p_1^2 > 0$ we must have $G^2 > \varepsilon^2$. For both G and ε positive the condition is just

$$G > \varepsilon. \tag{30}$$

Therefore, if $G > \varepsilon$ there is a family of equilibrium points that bifurcates from the origin at $G = \varepsilon$. It is easy to check from Eqs. (28) and (22) that

$$q_1^2 + p_1^2 = \frac{2J(G^2 - \varepsilon^2)}{G^2} = R_1^2 \tag{31}$$

$$q_2^2 + p_2^2 = \frac{J(G^2 - \varepsilon^2)}{\varepsilon^2 G^2} = R_2^2, \tag{32}$$

which means that this family projects as a circle on both (q_1, p_1) and (q_2, p_2) planes.

The energy value of those points is obtained by substituting these solutions into the Hamiltonian. The energy of the origin is obviously $E_0 = -J\varepsilon$. The points on the circle all have the same energy

$$E_c = -\frac{J}{2\varepsilon G^2}(G^4 + \varepsilon^4). \tag{33}$$

It is clear then (and it can be checked) that the origin becomes a saddle point at $G = \varepsilon$ and a valley of degenerate equilibria bifurcates.

(B) $G' \neq 0$

When G' is non-zero, it is not possible to find exact solutions of Eqs. (24)–(27) for both $q_1 \neq 0$ and $p_1 \neq 0$. However, the following two solutions do exist:

The p solution. $q_1 = q_2 = 0$ with p_1 and p_2 given by

$$p_1 = \pm \sqrt{2J(G_+^2 - \varepsilon^2)/G_+^2}$$
$$p_2 = \mp \sqrt{J(G_+^4 - \varepsilon^4)/G_+ \varepsilon^2}. \tag{34}$$

The corresponding energy is $E_p = -(J/2\varepsilon G_+^2)(G_+^4 + \varepsilon^4)$.

The q solution. $p_1 = p_2 = 0$ with q_1 and q_2 is given by

$$q_1 = \pm \sqrt{2J(G_-^2 - \varepsilon^2)/G_-^2}$$
$$q_2 = \mp \sqrt{J(G_-^4 - \varepsilon^4)/G_- \varepsilon^2}, \tag{35}$$

whose energy is $E_q = -(J/2\varepsilon G_-^2)(G_-^4 + \varepsilon^4)$.

It is clear from the above equations that the p-solution exists only if $G_+ > \varepsilon$ and the q-solution if $G_- > \varepsilon$ (we assume throughout the paper that G and G' are positive). A detailed discussion of stability of these solutions has been given elsewhere [9]. Here we summarize the results: When $G' = 0$ and $G < \varepsilon$ the only equilibrium point is the origin. As G is increased beyond ε the origin becomes a saddle point and a stable circle of equilibria arises. Next, when G' is turned on only four points on the circle remain: the p-solution which corresponds to a minimum and the q-solution which corresponds to a saddle point. As G' is further increased G_- will eventually become greater than ε and the q-solution will coalesce with the origin. If G' is nonzero from the beginning, the circle will not be seen and, when G and G' are changed, the origin bifurcates first into the p-solution and then into the q-solution.

4. Linear Analysis and Families of Periodic Orbits

The linear analysis of the equations of motion around the equilibrium points of the Hamiltonian is one of the most valuable methods for searching periodic orbits. We therefore start this section by presenting the linear solutions we shall need for our numerical studies. Throughout this section we consider the case where $\varepsilon = 1$ and $J = 9/2$.

4.1. *Linear Analysis*

The origin. In this case the equilibrium point corresponds to

$$q_1(t) = p_1(t) = q_2(t) = p_2(t) = 0.$$

The energy of this point is $E = -4.5$. Linearizing Eqs. (20)–(23) around this point we obtain

$$\dot{p}_1 \approx q_1 + G_- q_2$$
$$\dot{q}_1 \approx -p_1 - G_+ p_2$$
$$\dot{p}_2 \approx q_2 + G_- q_1 \tag{36}$$
$$\dot{q}_2 \approx -q_2 + G_+ p_1.$$

Defining the normal mode coordinates by

$$\begin{aligned} p_{\pm} &= p_1 \pm p_2 \\ q_{\pm} &= q_1 \pm q_2, \end{aligned} \tag{37}$$

Eqs. (36) decouple into

$$\begin{aligned} \dot{p}_+ &= (1+G_-)q_+ \\ \dot{q}_+ &= -(1+G_+)p_+ \\ \dot{p}_- &= (1-G_-)q_- \\ \dot{q}_- &= -(1-G_+)p_- \end{aligned} \tag{38}$$

which represent two decoupled oscillators with frequencies

$$\begin{aligned} \omega_+^2 &= (1+G_-)(1+G_+) \\ \omega_-^2 &= (1-G_-)(1+G_+). \end{aligned} \tag{39}$$

Let us write the Hamilton equations for the four-vector X given by

$$X = \begin{pmatrix} p_1 \\ p_2 \\ q_1 \\ q_2 \end{pmatrix} \tag{40}$$

in the usual symplectic way,

$$\dot{X} = \Lambda \nabla H_{cl} \tag{41}$$

If $X_0(t)$ is a periodic orbit, its stability is determined by the behaviour of nearby trajectories. The following construction is suitable for this investigation. Take

$$X = X_0 + \zeta. \tag{42}$$

Then to first order in ζ one has

$$\dot{\zeta} = \Lambda H'' \zeta, \tag{43}$$

where

$$H''_{ij} = \left. \frac{\partial^2 H''}{\partial X_i \, \partial X_j} \right|_{X = X_0}. \tag{44}$$

If H'' is time-independent, Eq. (43) can be integrated and gives

$$\zeta(t) = e^{\Lambda H'' t} \zeta(0) = M(t)\zeta(0). \tag{45}$$

The eigenvalues λ of $\Lambda H''$ are the *Liapunov exponents* and $e^{\lambda T}$ are the eigenvalues of the *Monodromy matrix* $M(T)$, where T is the period of the corresponding periodic orbit.

It is easy to compute $\Lambda H''$ in the limit of small q's and p's and the result is

$$\Lambda H'' = \begin{pmatrix} 0 & 0 & 1 & G_- \\ 0 & 0 & G_- & 1 \\ -1 & -G_+ & 0 & 0 \\ -G_+ & -1 & 0 & 0 \end{pmatrix} \tag{46}$$

with eigenvalues given by

$$\lambda = \begin{cases} \pm \imath\omega_+ = \pm \imath \sqrt{(1+G_+)(1+G_-)} \\ \pm \imath\omega_- = \pm \imath \sqrt{(1-G_+)(1-G_-)}. \end{cases} \tag{47}$$

To study the stability of periodic orbits in two degrees of freedom systems, it is enough to calculate the trace of their monodromy matrices [12, 13]:

$$\mathrm{tr}(M) = e^{\imath\omega_- T} + e^{-\imath\omega_+ T} + e^{\imath\omega_- T} + e^{-\imath\omega_- T} = 2(\cos\omega_+ T + \cos\omega_- T). \tag{48}$$

The p-solutions. The linearization around the p-points (Eq. (34)) are also straightforward and lead to the equations

$$\begin{aligned} \dot{p}_1 &\approx \gamma_+^2 q_1 + \frac{G_-\gamma}{G_+} q_2 \\ \dot{q}_1 &\approx -\frac{G_+''}{\gamma_+^2} p_1 - \frac{p_2}{\gamma_+} \\ \dot{p}_2 &\approx q_2 + \frac{G_-\gamma}{G_+} q_1 \\ \dot{q}_1 &\approx -p_2 - \frac{p_1}{\gamma_+}, \end{aligned} \tag{49}$$

where $\gamma_+ = \sqrt{(G_+^2+1)/2}$.

The above equations do not decouple as easily as before. Rewriting the equation in the form

$$\begin{pmatrix} \ddot{q}_1 \\ \ddot{q}_2 \end{pmatrix} = -\begin{pmatrix} G_+^4 + \dfrac{G_-}{G_+} & \dfrac{1+G_-G_+^3}{\gamma_+} \\ \gamma_+\left(1+\dfrac{G_-}{G_+}\right) & 1+\dfrac{G_-}{G_+} \end{pmatrix} \begin{pmatrix} q_1 \\ q_2 \end{pmatrix} \equiv -\Omega^2 \begin{pmatrix} q_1 \\ q_2 \end{pmatrix}, \tag{50}$$

it is now easy to obtain the eigenvalues (from (50)) and we shall use the result in the next section.

4.2. *Families of Periodic Orbits*

The classical limit of the Dicke Maser model, Eq. (18), does not display the usual form, a kinetic energy term which depends only on the momenta plus a coordinate dependent potential. This is due to the presence of the spin degree of freedom. Note in particular that the spin space (p_1, q_1) is finite and limited to the circle $p_1^2 + q_1^2 \leqslant 4J$. A periodic orbit exists precisely at the border of this circle, as can be checked from the equations of motion, for $p_2 = q_2 = 0$ and energy $E = J$. We call this solution the *border solution*. It is given by

$$\begin{aligned} q_1(t) &= -\sqrt{4J}\sin t \\ p_1(t) &= \sqrt{4J}\cos t. \end{aligned} \tag{51}$$

Other more complex p.o. can only be obtained numerically. For such purposes it is necessary to have a method that is capable of treating general analytic Hamiltonians. In Appendix A we present an extension of the method developed in Ref. [8] in order to treat our Hamiltonian.

The main purpose of the discussion which follows is to exploit the novel effects coming from the spin degree of freedom. In particular we wish to comprehend the consequences of both the presence of the border and chaos. The former should be apparent even in the integrable regime $(G' = 0)$.

According to the Liapunov–Weinstein theorem [14] there exist two families of periodic solutions of the full system that behave harmonically as their amplitudes go to zero. The "seeds" of nonlinear solutions are then small amplitude solutions. We call the families originating at these "seeds" DIAGP and DIAGM. These names

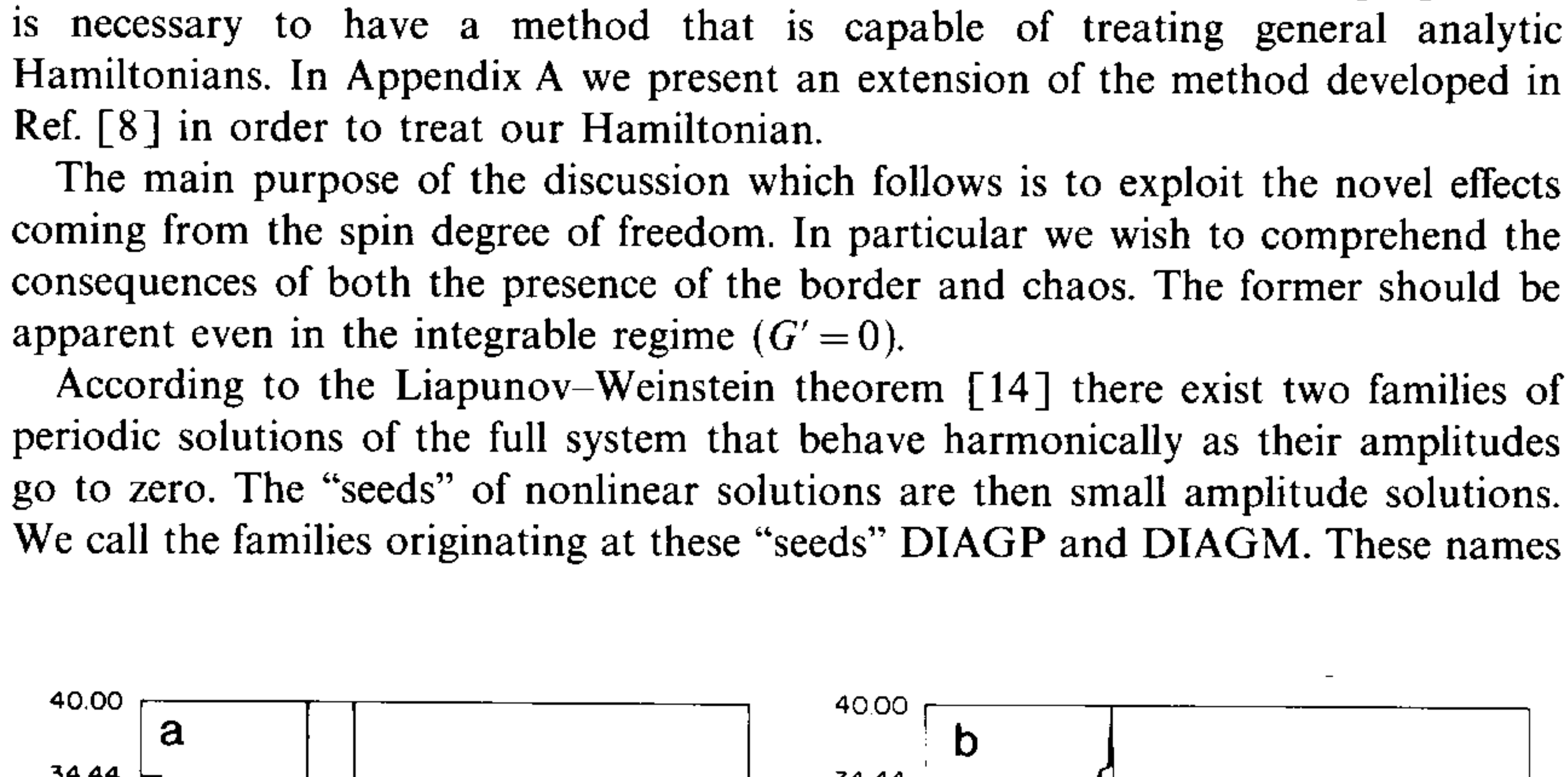

FIG. 1. Energy versus period for the simplest families of periodic orbits. (a) The coupling parameters are $G = 0.5$, $G' = 0.2$. (b) Thick (thin) lines correspond to stable (unstable) orbits. The coupling parameters are $G = 0.5$, $G' = 0.2$.

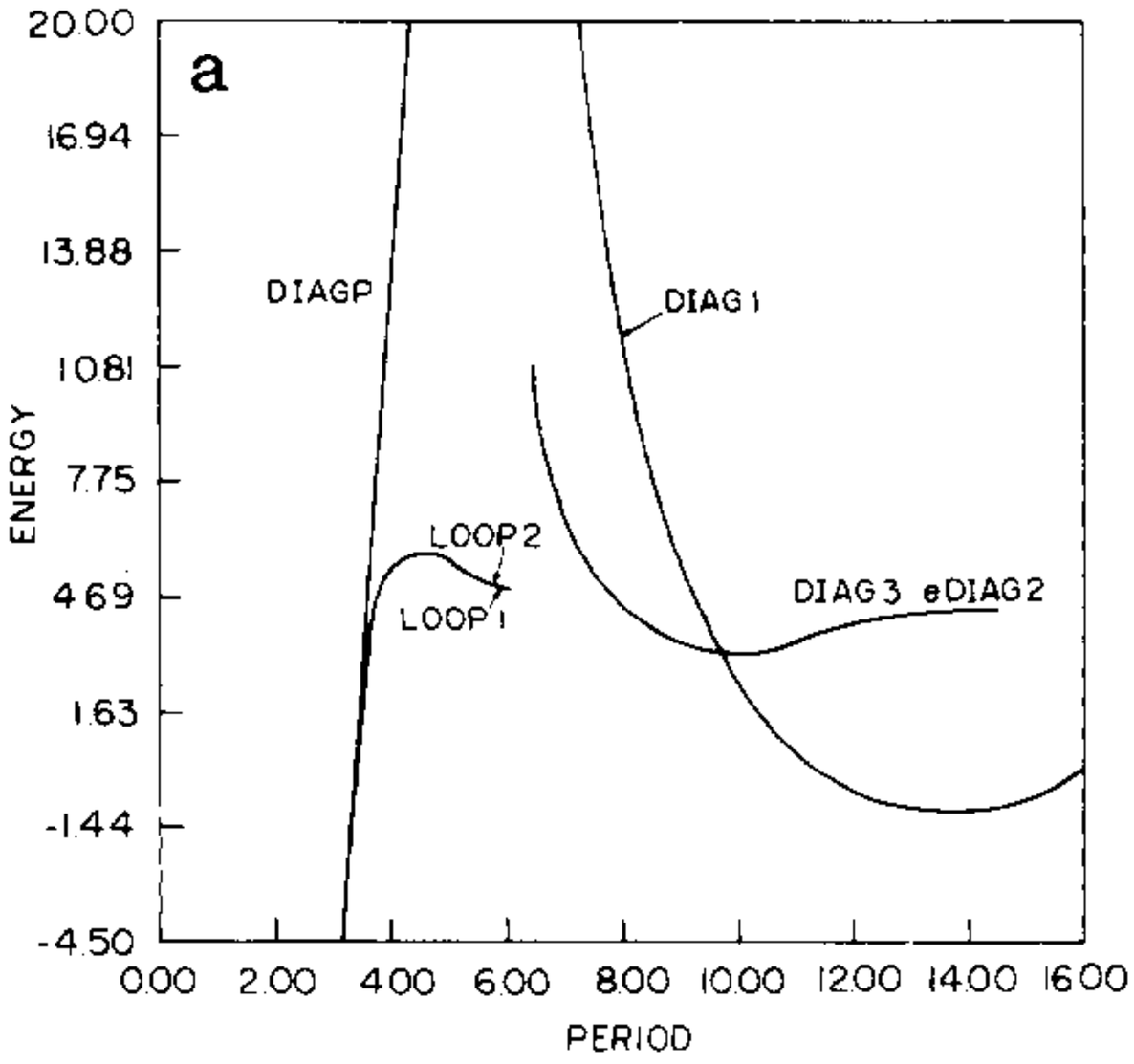

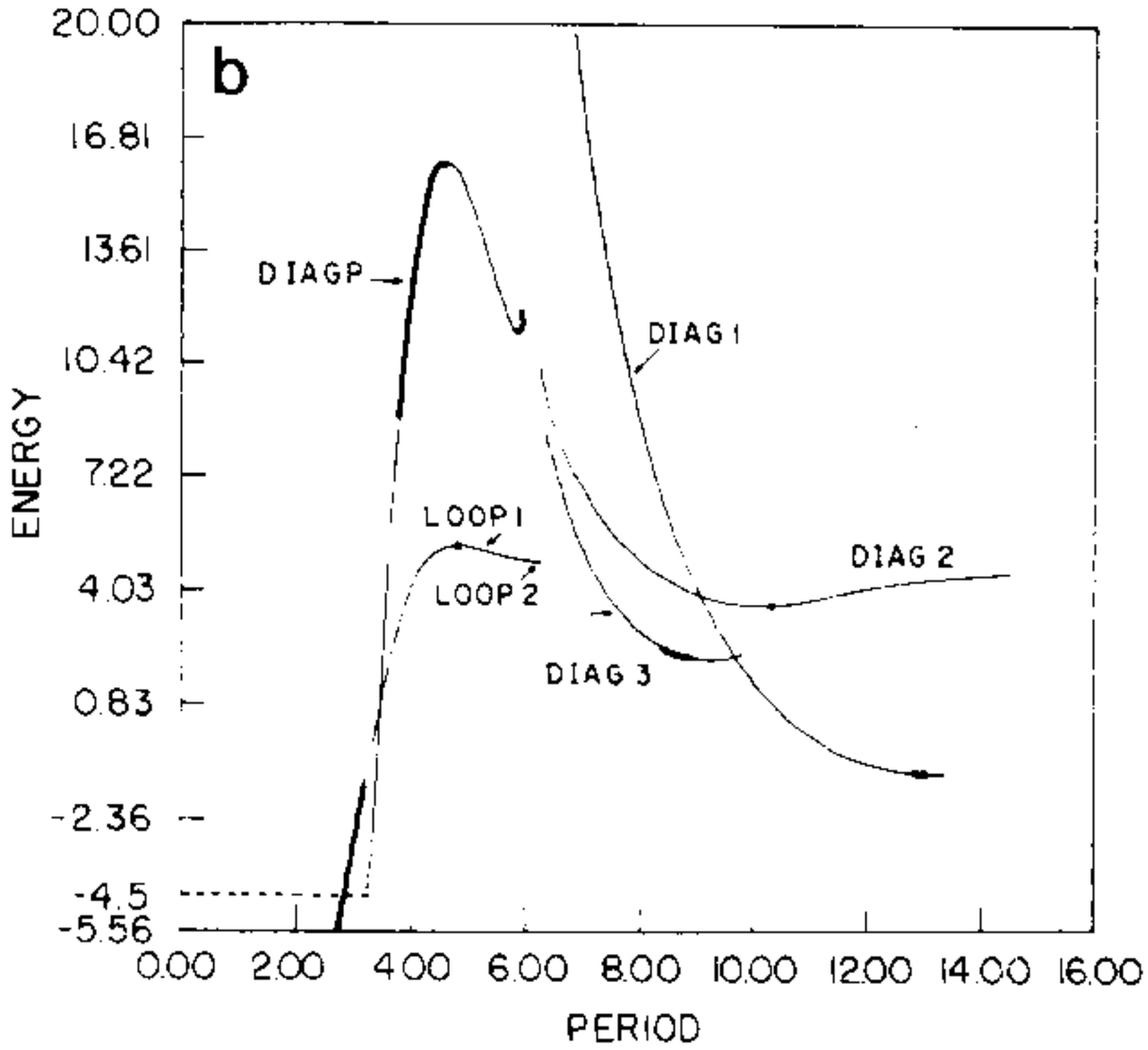

FIG. 2. (a) Same as Fig. 1a for $G = 1.0$, $G' = 0.0$. (b) Same as Fig. 1b for $G = 1.0$, $G' = 0.4$.

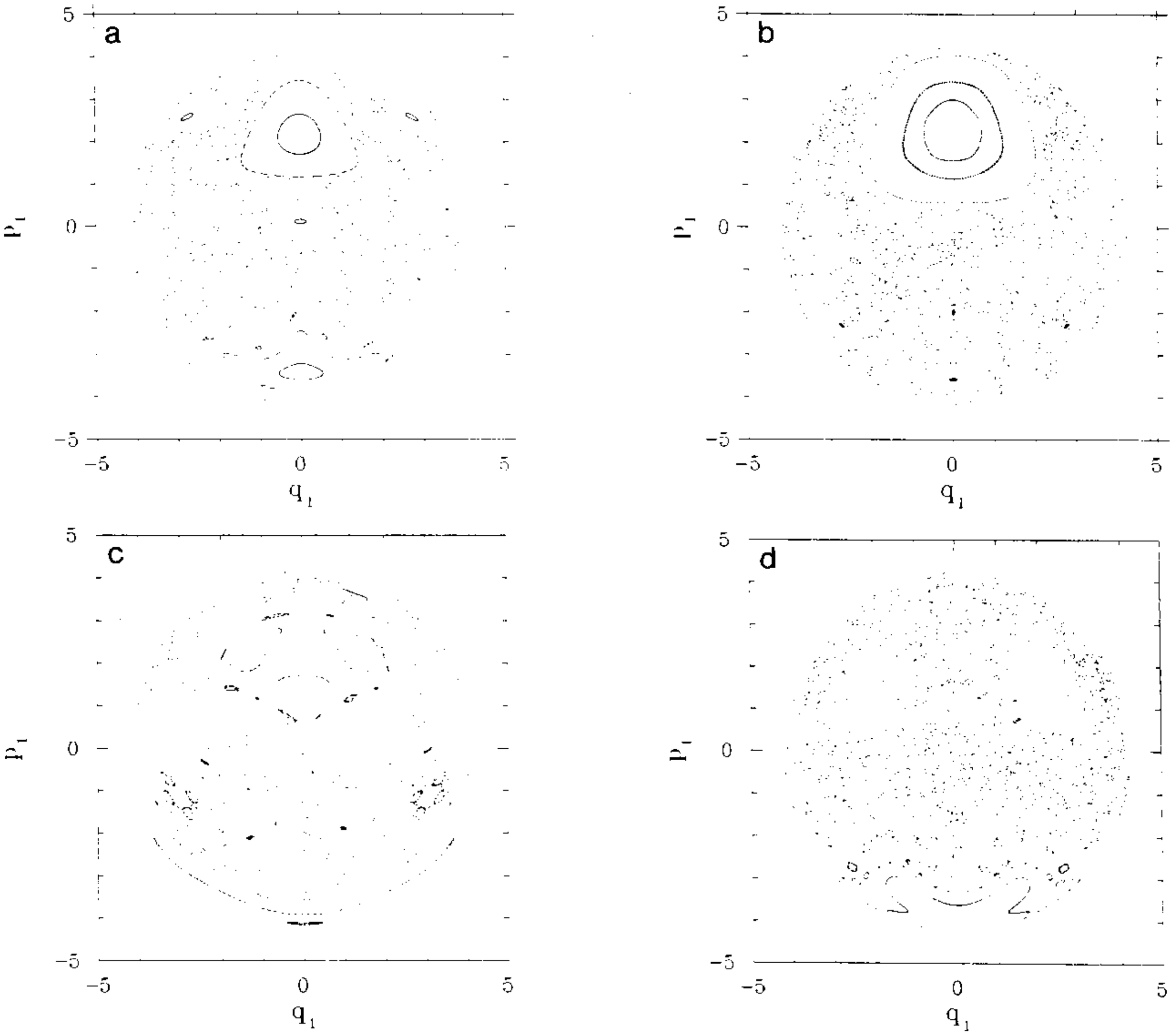

FIG. 3. Poincaré section of the spin degree of freedom (at $q_2 = 0$). The parameter values are $G = 0.5$, $G' = 0.2$. The precision in energy is $\delta E/E_0 = 10^{-5}$ in all the cases: (a) total energy $E_0 = 6.2$; (b) total energy $E_0 = 8.5$; (c) total energy $E_0 = 15$; (d) total energy $E_0 = 25$.

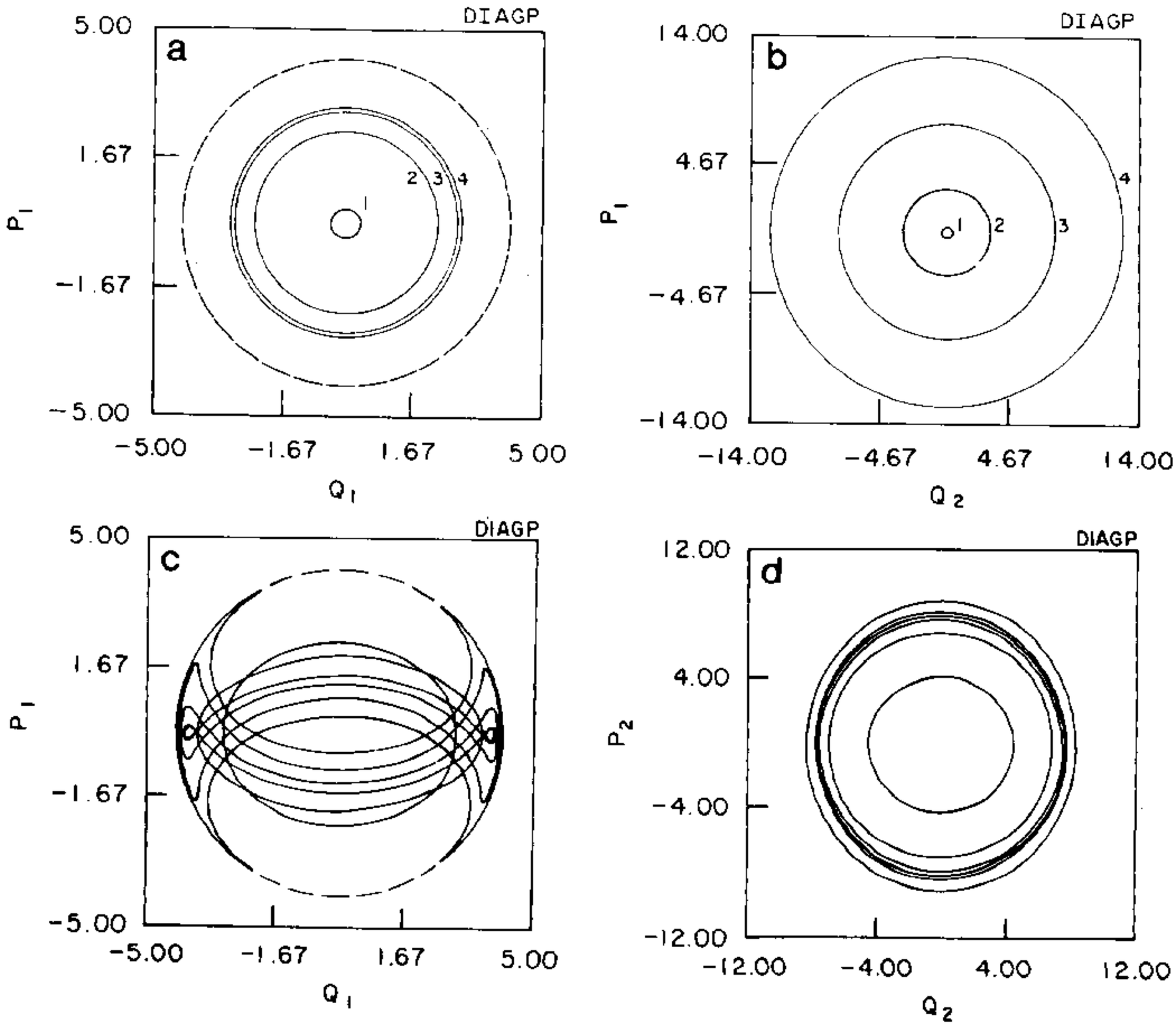

FIG. 4. (a) Sequence in energy of projections of periodic orbits from the family DIAGP in the plane (p_1, q_1) for the parameter values in Fig. 1a. (b) Same for the $p_2 \times q_2$ projection. (c) Same as Fig. 4a for the parameter values of Fig. 1b. (d) Same as Fig. 4b for the parameter values in Fig. 1b.

are related to the fact that the normal modes solutions (Eqs. (37)) correspond to diagonal oscillators in the first-to-third and second-to-fourth quadrants in the plane (q_1, q_2), respectively.

Periodic orbits generically form one-parameter families. The parameter is usually chosen to be the energy or the period. Figures 1 and 2 show the Energy × Period ($E \times \tau$) plot of families DIAGP, DIAGM, and others. In this plot the families are represented by curves, each point being a periodic orbit with given energy and period.

As discussed in Section 3 we will have at least two families of periodic orbits which start from the points of minima. Moreover, there will be a bifurcation of minima as the sum of the coupling constants $G + G'$ is increased [9]. We therefore choose four sets of parameter values that correspond to both situations in the integrable (i) and non integrable (ni) cases

$$\text{SET1} \begin{cases} \text{(i)} & G = 0.5, \quad G' = 0 \\ \text{(ni)} & G = 0.5, \quad G' = 0.2 \end{cases} \tag{52}$$

$$\text{SET2} \begin{cases} \text{(i)} & G = 1.0, \quad G' = 0 \\ \text{(ni)} & G = 1.0, \quad G' = 0.4. \end{cases} \tag{53}$$

The families of p.o. for the first set of parameters are shown in Fig. 1a (i) and Fig. 1b (ni). DIAGP corresponds to the "seed" with the smaller period (obtained from (39)) and is present in both cases. In Fig. 1a the corresponding orbits will show clearly the border effects (projections in the planes (p_1, q_1) and (p_2, q_2) are circles, in the integrable case, as expected). The radii of the circles increase with increasing energy in both trajectories. The effect of the border in the spin degree of freedom is most clearly seen for energies such that the corresponding p.o. projection approaches the border. In this case the radius of the particle p.o. projection increases much more rapidly with increasing energy as compared to the spin p.o. projection. This suggests that, as the energy is increased, the presence of the border favours the concentration of the energy in the particle degree of freedom. This result is qualitatively maintained for the second set of parameter values when chaos is present. The presence of chaos can be best visualized with a Poincaré section. Figure 3 shows the Poincaré section for the parameter values in SET1 that correspond to the nonintegrable case (ni) [15]. The form of the p.o. projections is also affected as can be seen in Figs. 4(a–d). The bonbon shaped curve in Fig. 4c starts precisely at the energy when the curve DIAGP (Fig. 1b) presents a wiggle. For the second set of parameter values (i) and (ni) these features are maintained, inspite of the fact that DIAGP in Fig. 2b starts at a saddle point (the origin).

In order to discuss the other three families of p.o. in Fig. 1a (note that DIAGM1 and DIAGM2 are degenerate), it is important to note that in this case we have $\omega_+/\omega_- = 3$. This can be seen from $H_{\rm cl}$ in terms of the action angle variables in Eq. (12). If $G' = 0$ only the combination of angles $(\theta_1 - \theta_2)$ appears in $H_{\rm cl}$, implying that $I_1 + I_2$ is constant. From Eq. (39) we have

$$\begin{aligned} \omega_+ &= 1 + G = \tfrac{3}{2} \\ \omega_- &= 1 - G = \tfrac{1}{2} \end{aligned} \tag{54}$$

which assume rational values whenever G is rational. In general, this is not true when $G' \neq 0$ as can be seen from Eq. (47). From Eq. (48),

$$\begin{aligned} \mathrm{tr}(M)_{\rm DIAGP} &= 2 + 2\cos(2\pi/3) = 1 \\ \mathrm{tr}(M)_{\rm DIAGM} &= 2 + 2\cos 6\pi = 1 \end{aligned} \tag{55}$$

are the zeroth order approximation for the trace of their monodromy matrix. In

---

FIG. 5. (a) Representative periodic orbit of the family DIAGM1 in Fig. 1a projected on the $(p_1 \times q_1)$ plane. (b) Same on the $(p_2 \times q_2)$ plane. (c) Representative periodic orbit of the family DIAGM2 in Fig. 1a projected on the $(p_1 \times q_1)$ plane. (d) Same on the $(p_2 \times q_2)$ plane. (e) Representative periodic orbit of the family DIAGM1 (right branch) in Fig. 1b projected on the $(p_1 \times q_1)$ plane. (f) Same on the $(p_2 \times q_2)$ plane. (g) Representative periodic orbit of the family DIAGM in Fig. 1b projected on the $(p_1 \times q_2)$ plane. (h) Same on the $(p_2 \times q_2)$ plane.

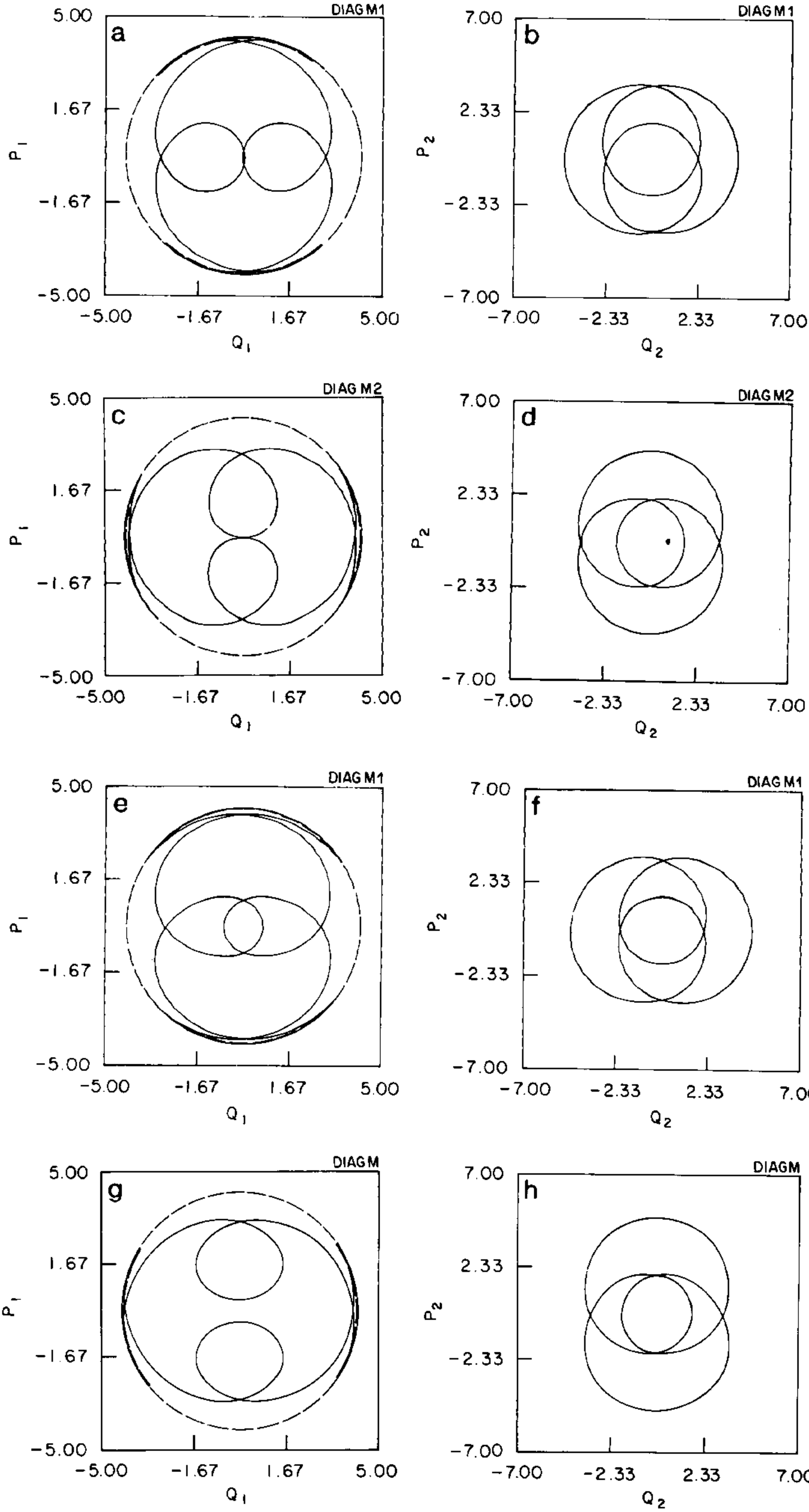
a
DIAG M1
5.00
1.67
-1.67
-5.00
P_1
-5.00
-1.67
1.67
5.00
Q_1
b
DIAG M1
7.00
2.33
-2.33
-7.00
P_2
-7.00
-2.33
2.33
7.00
Q_2
c
DIAG M2
5.00
1.67
-1.67
-5.00
P_1
-5.00
-1.67
1.67
5.00
Q_1
d
DIAG M2
7.00
2.33
-2.33
-7.00
P_2
-7.00
-2.33
2.33
7.00
Q_2
e
DIAG M1
5.00
1.67
-1.67
-5.00
P_1
-5.00
-1.67
1.67
5.00
Q_1
f
DIAG M1
7.00
2.33
-2.33
-7.00
P_2
-7.00
-2.33
2.33
7.00
Q_2
g
DIAG M
5.00
1.67
-1.67
-5.00
P_1
-5.00
-1.67
1.67
5.00
Q_1
h
DIAG M
7.00
2.33
-2.33
-7.00
P_2
-7.00
-2.33
2.33
7.00
Q_2

this particular case ($G=0.5$), we have a rotational torus of the p.o. solution given by the normal modes, Eq. (37),

$$p_1 = A_+ \sin\frac{3t}{2} + A_- \sin\frac{t}{2}$$

$$q_1 = A_+ \cos\frac{3t}{2} + A_- \cos\frac{t}{2} \tag{56}$$

$$p_2 = A_+ \sin\frac{3t}{2} - A_- \sin\frac{t}{2}$$

$$q_2 = A_+ \cos\frac{3t}{2} - A_- \cos\frac{t}{2}$$

for each choice of nonzero pairs (A_+, A_-). The period of the degenerate p.o. filling the torus is $\tau = 4\pi$ and in the $E \times \tau$ plot it is represented by a single point in the degenerate curves DIAGM1 and DIAGM2. As the energy tends to the lowest value of $E = -4.5$, all the degenerate tori merge in the phase space to the vicinity of the origin $q_1 = p_1 = q_2 = p_2 = 0$. In particular, $A_- = 0$ corresponds to the limit, where the torus is reduced to the family of p.o. DIAGP, and $A_+ = 0$ to the family of p.o. DIAGM. When G' is switched on (see Fig. 1b), the system becomes nonintegrable and the rational torus breaks down in a very peculiar way: the periodic orbits which survive the torus destruction constitute a single family, DIAGM1, that emerges at an energy larger than the minimum in a "U" shaped form in the $E \times \tau$ plot (see Fig. 1b). The right branch is unstable (thin line) and the left one is stable (full line). The normal oscillation DIAGM bends very quickly towards higher periods and the global picture looks as though the old DIAGM of the integrable case has split into the left branch of DIAGM1 plus the low energy part of DIAGM.

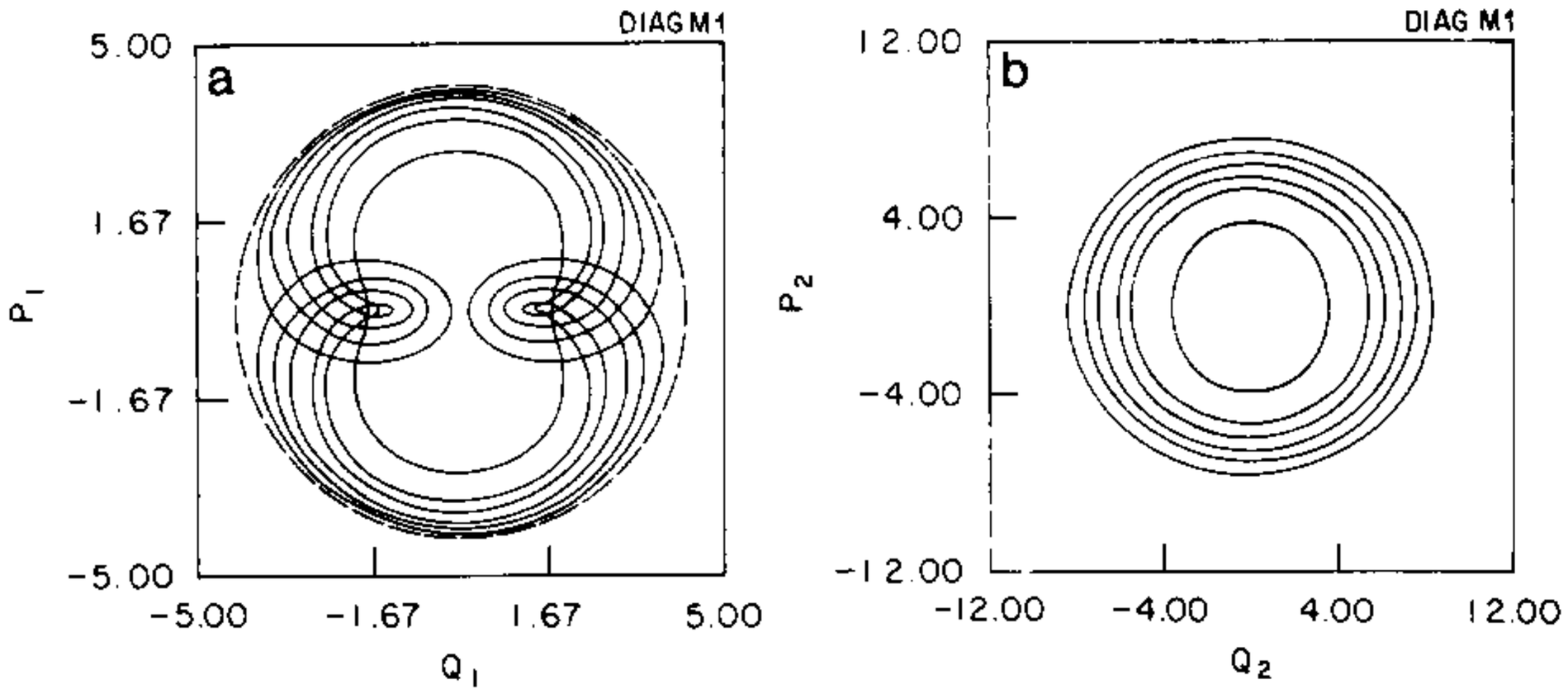

FIG. 6. (a) Sequence (with increasing energy) of periodic orbits of the left branch of the family DIAGM1 in Fig. 1b projected on the $(p_1 \times q_1)$ plane. (b) Same for the $(p_2 \times q_2)$ projection.

Also the old degenerate curves DIAGM1 and DIAGM2 seem to have broken into the right branch of DIAGM1 plus the high energy part of DIAGM. The typical p.o. projections of set 1 (i) and (ni) for DIAGM1 (right branch) and DIAGM2 and DIAGM are shown in Figs. 5a–h. As can be observed, the chaotic regime has the effect of slightly distorting the trajectories. These families maintain their energy around 6.2 as the period increases. The shapes wih increasing period are essentially maintained also (see Fig. 5). A sequence of projections of p.o. from DIAGM1 set 1 (ni) (left branch) are shown in Figs. 6a and b.

The second set of parameters, Eq. (53), presents a novel family which arises due to the phase transition, LOOP1. The name comes from the fact that its small amplitude orbit on the (q_1, q_2) plane has approximately the form of an eight. As discussed before two "seeds" are expected in this case too. The second seed actually exists (see Fig. 2), but numerical difficulties prevented us from calculating the corresponding family. When $G' = 0$ (see Fig. 2a) we are precisely at the transition point and the origin is a minimum. Note that inspite of this fact the LOOP1 family

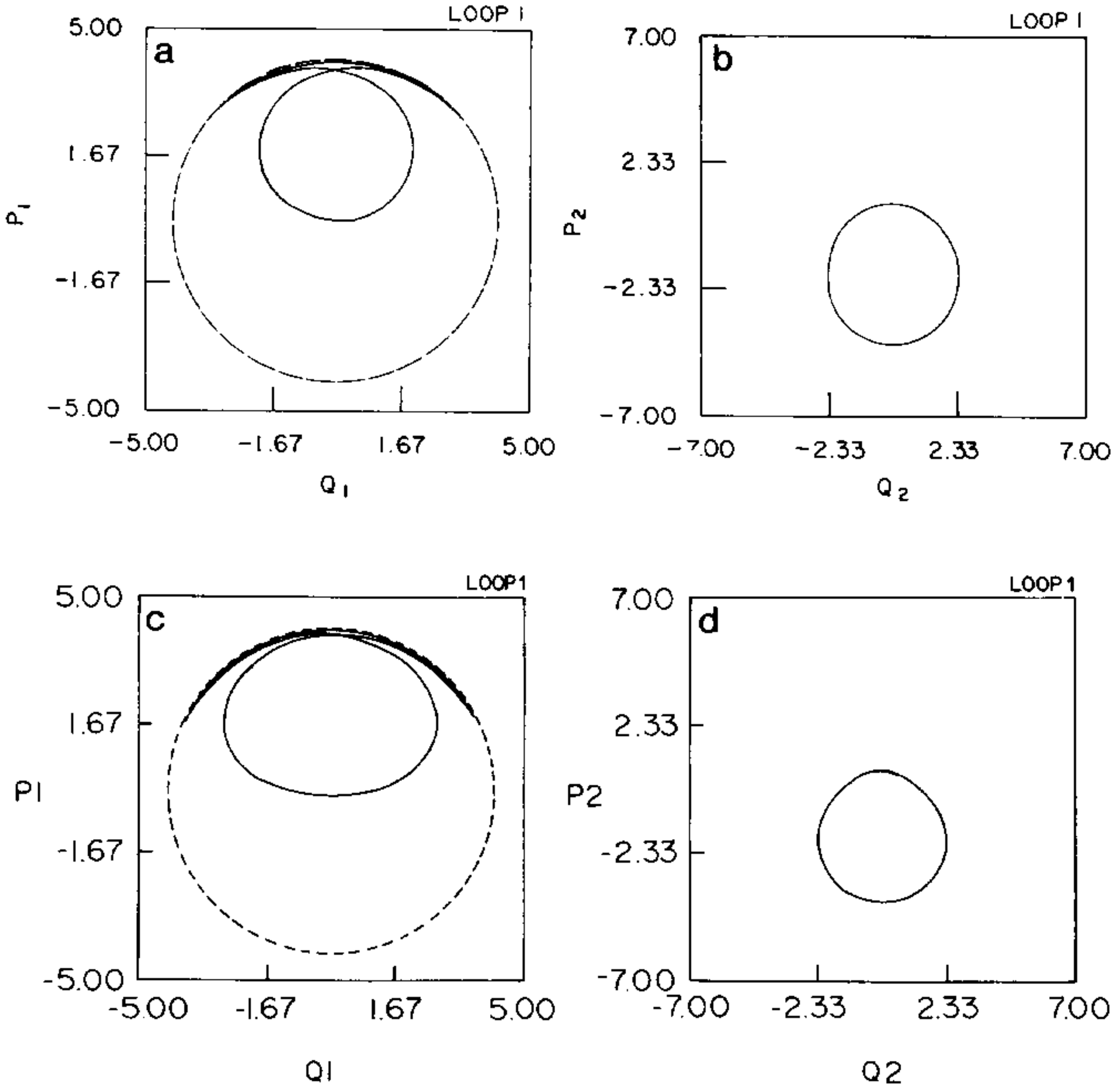

FIG. 7. (a) Representative periodic orbit of the family LOOP1 in Fig. 2a projected on the $(p_1 \times q_1)$ plane. (b) Same on the $(p_2 \times q_2)$ plane. (c) Representative periodic orbit of the family LOOP1 in Fig. 2b projected on the $(p_1 \times q_1)$ plane. (d) Same on the $(p_2 \times q_2)$ plane.

is present. The second seed, in this case goes to infinity (as can be verified from the solution of Eq. (50)).

The typical p.o. projections of the family LOOP1 are shown in Figs. 7a–d. It is interesting to notice that families LOOP1 and LOOP2 are the only ones we have which present nonsymmetrical solutions in both projections (the family LOOP2 shows a complementary behaviour to LOOP1). The effect of chaos is, as in the other cases, to deform the orbits slightly. The family DIAG1 in Fig. 2b is similar to the family DIAGM1 in Fig. 1b (left branch), though much more unstable. The same does not happen in the integrable case, perhaps due to the fact that this case is very special in the sense that one is precisely at the transition point. The family DIAG2 in Fig. 2b was obtained by numerical search using orbits from Fig. 1b. An interesting case are the families DIAG1 as compared to DIAG3 and DIAG2 in Figs. 2a and b. The typical p.o. projections from DIAG1 look like a superposition of p.o. projections from DIAG3 and DIAG2 (see Figs. 8a–l). Chaos in this case has a larger deformation effect on the integrable orbits, as expected. Also all the families of p.o. present much more unstable orbits as compared to the families in Fig. 1b.

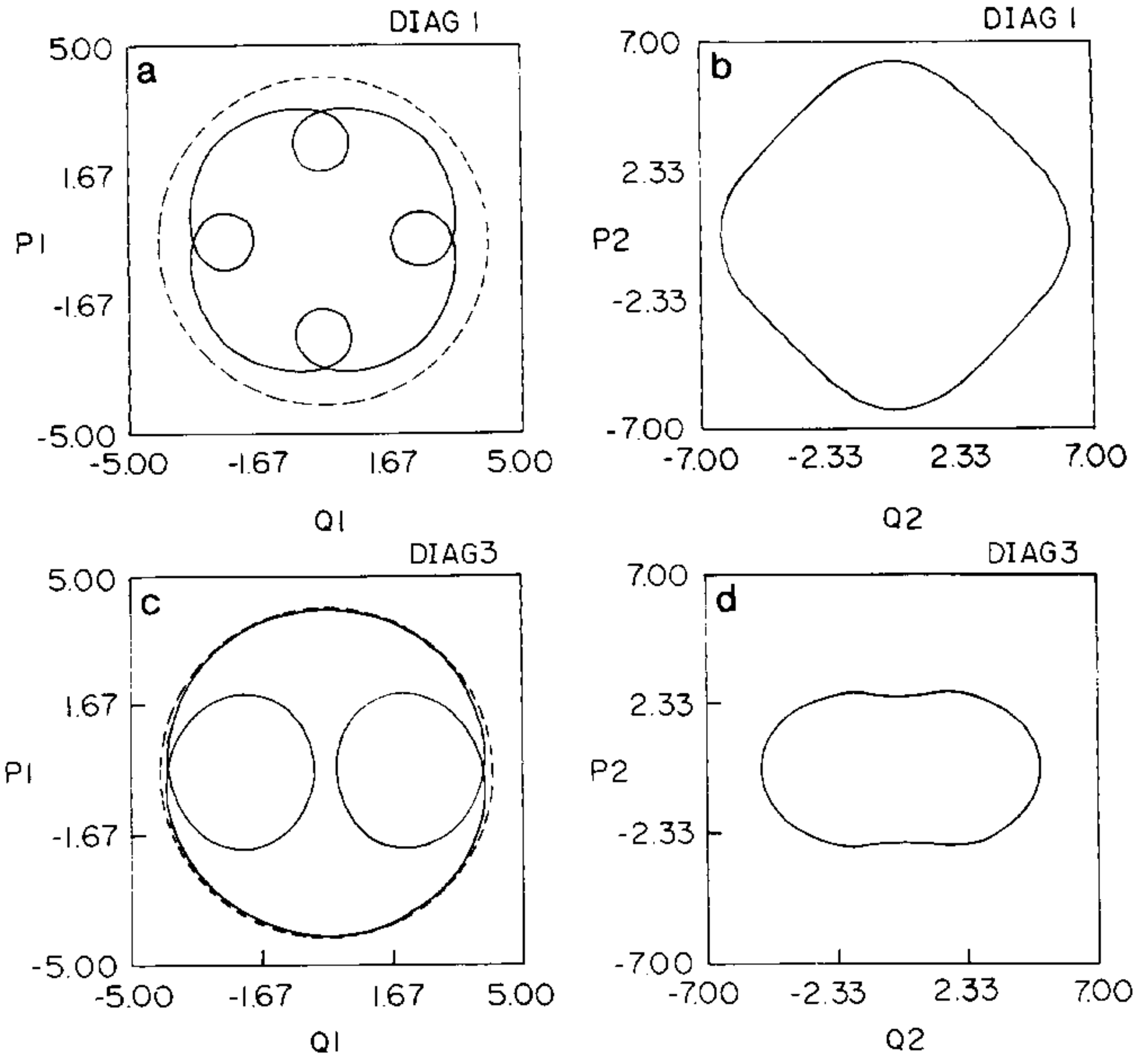

FIG. 8. (a) Representative periodic orbit of the family DIAG1 in Fig. 2a projected on the $(p_1 \times q_2)$ plane. (b) Same on the $(p_2 \times q_2)$ plane. (c) Representative periodic orbit of the family DIAG3 in Fig. 2a projected on the $(p_1 \times q_1)$ plane. (d) Same on the $(p_2 \times q_2)$ plane. (e) Representative periodic orbit of the family DIAG2 in Fig. 2a projected on the $(p_1 \times q_1)$ plane. (f) Same on the $(p_2 \times q_2)$ plane. (g)–(l) Same as Figs. 8a–f with the parameter values of Fig. 2b.

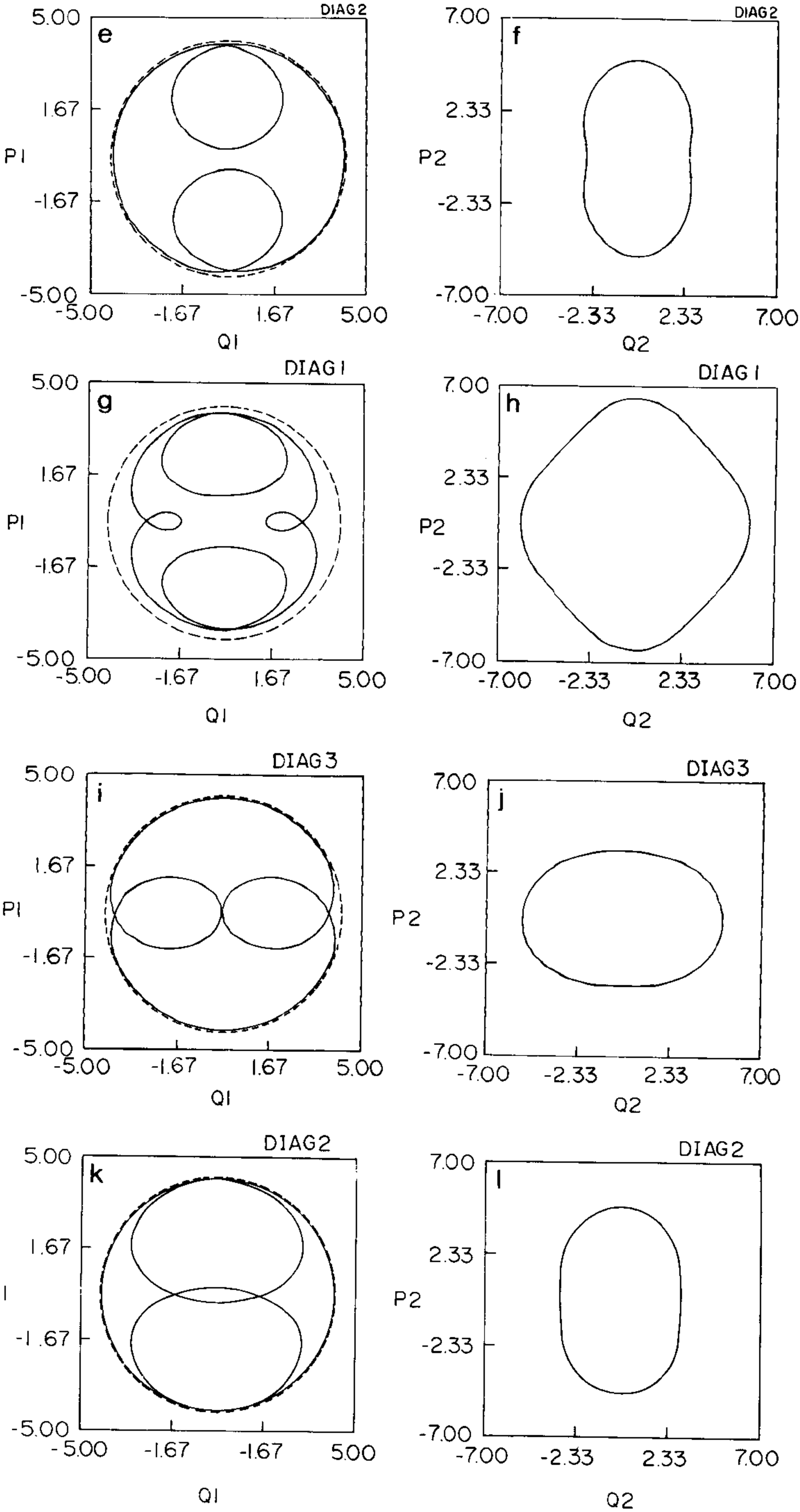

FIGURE 8—*Continued*

5. Concluding Remarks

In the present work we have extensively exploited the behaviour of periodic orbits in the classical limit of the Dicke Maser model. In particular, as the model exhibits a phase transition we investigated its influence on the orbits in both regimes, integrable and nonintegrable. The finiteness of the spin phase space was shown to have a strong influence on the systematic behaviour of p.o. as a function of energy for various families. In order to complete this numerical study we investigate, in the following contribution, the connection of our classical results with the quantum eigenfunctions of the model, especially focusing on the presence of scars and how they can be affected by border effects and chaotic classical dynamics.

APPENDIX A: Numerical Calculation of Periodic Orbits

In this appendix we extend the "monodromy method" developed by Baranger *et al.* [8] for Hamiltonians of the form

$$H(\mathbf{p}, \mathbf{q}) = \frac{\mathbf{p}^2}{2} + V(\mathbf{q})$$

to general analytic Hamiltonians. The technique is based on Newton's method and, therefore we start by giving a (discretized) guess for the periodic solution we are looking for. Let $\{p^0_{1n}, p^0_{2n}, q^0_{1n}, q^0_{2n}\}$ with $n = 1, 2, ..., N'$ and $p^0_{1\,N+1} = p^0_{1\,1}$, etc. be such a guess. The points on the orbit will be assumed to be spaced in time with time step ε' and period $T = N'\varepsilon'$. The time derivative is then defined in a symmetric way:

$$\dot{f}(t) = \frac{df}{dt} \to \frac{1}{2}\left[\frac{f_{n+1} - f_n}{\varepsilon'} + \frac{f_n - f_{n-1}}{\varepsilon'}\right] = \frac{f_{n+1} - f_{n-1}}{2\varepsilon'}. \tag{57}$$

With the help of the four-vector

$$X = \begin{pmatrix} p_1 \\ p_2 \\ q_1 \\ q_2 \end{pmatrix}, \tag{58}$$

we define the value of $f(X)$ at $t = n\varepsilon$ as

$$f(X(t)) \to f\left(\frac{X_{n+1} + X_{n-1}}{2}\right). \tag{59}$$

With these definitions, Hamilton's equations take the discrete form

$$X_{n+1} = X_{n-1} + 2\varepsilon' \Lambda \nabla H \left(\frac{X_{n+1} + X_{n-1}}{2} \right), \tag{60}$$

where

$$\Lambda = \begin{pmatrix} 0 & 0 & 1 & 0 \\ 0 & 0 & 0 & 1 \\ -1 & 0 & 0 & 0 \\ 0 & -1 & 0 & 0 \end{pmatrix}. \tag{61}$$

Assuming N' even we can relabel the points and obtain

$$X_{n+1} = X_n + \varepsilon \Lambda \nabla H \left(\frac{X_n + X_{n+1}}{2} \right), \tag{62}$$

where

$$\begin{aligned} &n = 1, 2, ..., N = N'/2, \\ &\varepsilon = 2\varepsilon', \\ &T = N'\varepsilon' = N\varepsilon. \end{aligned} \tag{63}$$

So, giving a trial solution $\{X_n^0\}_{n=1,...,N}$ we construct

$$X_n = X_n^0 + X_n', \tag{64}$$

substitue (64) into (62), and expand to first order in X_n' to obtain

$$X'_{n+1} = U_n X_n' + C_n, \tag{65}$$

where

$$\begin{aligned} U_n &= \left(1 - \frac{\varepsilon}{2} \Lambda \bar{H}_n'' \right)^{-1} \left(1 + \frac{\varepsilon}{2} \Lambda \bar{H}_n'' \right) \\ C_n &= \left(1 - \frac{\varepsilon}{2} \Lambda \bar{H}_n'' \right)^{-1} (X_{n+1}^0 - X_n^0 - \varepsilon \Lambda \nabla \bar{H}_n^0) \\ (\bar{H}_n'')_{ij} &= \left. \frac{\partial^2 H}{\partial X_i \, \partial X_j} \right|_{(X_n^0 + X_{n+1}^0)/2} \\ \bar{\nabla} \bar{H}_n^0 &= \nabla H \left(\frac{X_n^0 + X_{n+1}^0}{2} \right). \end{aligned} \tag{66}$$

Equation (65) can be iterated, yielding

$$X'_{N+1} = M_1 X_1' + B_1, \tag{67}$$

where

$$M_1 = U_N U_{N-1} \cdots U_2 U_1$$
$$B_1 = U_N U_{N-1} \cdots U_2 C_1 + U_N U_{N-1} \cdots U_3 C_2 + \cdots + U_N C_{N-1} + C_N. \tag{68}$$

Imposing that the new solution $\{X_n\}$ be periodic, $X_{N+1} = X_1$, and using the fact that $\{X_n^0\}$ is periodic by construction, we find that $X'_{N+1} = X'_1$. Therefore, (67) yields

$$X'_1 = (1 - M_1)^{-1} B_1. \tag{69}$$

The other X'_n can then be calculated with the help of (65) and the whole process iterated until the desired precision.

It should be noted that the more naive version of the time derivative $\dot{f}(t) \to (f_{n+1} - f_n)/\varepsilon$ results in a very unstable algorithm that barely works for nearly linear systems. The symmetrized form used here guarantees invariance by time-reversion when this symmetry exists in the problem, resulting in a very powerful method. As in Baranger's method, both stable and unstable orbits can be followed, and we refer to the original paper [4] for a detailed discussion of how to use and how to get started, using the "monodromy method."

REFERENCES

1. R. H. DICKE, *Phys. Rev.* **93** (1954), 99.
2. K. HEPP AND E. H. LIEB, *Ann. Phys. (N.Y.)* **76** (1973), 360.
3. R. GRAHAM AND M. HÖHNERBACH, *Z. Phys. B* **57** (1984), 233.
4. M. B. CIBILS *et al.*, *J. Phys. A* **23** (1990), 545.
5. F. T. ARECCHI AND E. COURTENS, *Phys. Rev. A* **2** (1970), 1730.
6. R. GRAHAM AND M. HÖHNERBACH, *Phys. Rev. Lett.* **57** (1986), 1378.
7. C. H. LEWENKOPF, M. C. NEMES, V. MARVULLE, M. P. PATO, AND W. F. WRESZINSKI, *Phys. Lett. A* **155** (1991), 113.
8. M. BARANGER, K. T. R. DAVIES, AND J. H. MAHONEY, *Ann. Phys. (N.Y.)* **186** (1988), 95.
9. M. A. M. DE AGUIAR, K. FURUYA, AND M. C. NEMES, *Quant. Opt.* **3** (1991), 305.
10. J. KURCHAN, P. LEBOEUF, AND M. SARRACENO, *Phys. Rev. A* **40** (1989), 6800.
11. P. KRAMER AND M. SARRACENO, Lecture Notes in Phys., Vol. 140, Springer-Verlag, New York, 1981.
12. V. A. YAKUBOVICH AND V. M. STARZHINKŬ, "Linear Differential Equations with Periodic Coefficients," Keter, Jerusalem, 1975.
13. M. A. M. DE AGUIAR *et al.*, *Ann. Phys.* **180** (1987), 167.
14. A. WEINSTEIN, *Invent. Math.* **20** (1973), 47.
15. K. FURUYA, M. A. M. DE AGUIAR, C. H. LEWENKOPF, AND M. C. NEMES, *Ann. Phys. (N.Y.)* **216** (1992), 313–322.

Printed by Catherine Press, Ltd., Tempelhof 41, B-8000 Brugge, Belgium